

UC Berkeley

UC Berkeley Previously Published Works

Title

Near-Field Nanoimaging of Phases and Carrier Dynamics in Vanadium Dioxide Nanobeams.

Permalink

<https://escholarship.org/uc/item/2gw6t0h3>

Journal

ACS Photonics, 11(8)

ISSN

2330-4022

Authors

Yang, Rundi

Li, Jingang

Cai, Yuhang

et al.

Publication Date

2024-08-21

DOI

10.1021/acsp Photonics.4c00848

Copyright Information

This work is made available under the terms of a Creative Commons Attribution-NonCommercial-NoDerivatives License, available at

<https://creativecommons.org/licenses/by-nc-nd/4.0/>

Peer reviewed

Near-Field Nanoimaging of Phases and Carrier Dynamics in Vanadium Dioxide Nanobeams

Rundi Yang,[§] Jingang Li,^{*,§} Yuhang Cai, Brian W. Blankenship, Junqiao Wu,^{*} and Costas P. Grigoropoulos^{*}



Cite This: *ACS Photonics* 2024, 11, 3359–3364



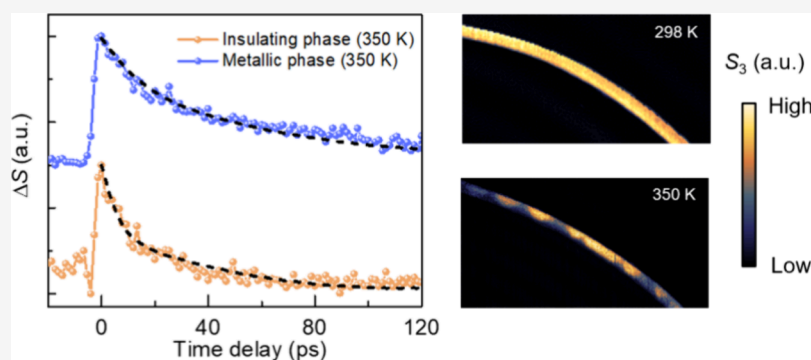
Read Online

ACCESS |

Metrics & More

Article Recommendations

Supporting Information



ABSTRACT: The stable coexistence of insulating and metallic phases in strained vanadium dioxide (VO_2) has garnered significant research interest due to the intriguing phase transition phenomena. However, the temporal behavior of charge carriers in different phases of VO_2 remains elusive. Herein, we employ near-field optical nanoscopy to capture nanoscale alternating phase domains in bent VO_2 nanobeams. By conducting transient measurements across the different phases, we observed a prolonged carrier recombination lifetime in the metallic phase of VO_2 , accompanied by an accelerated diffusion process. Our findings reveal nanoscale carrier dynamics in VO_2 nanobeams, offering insights that can facilitate further investigations into phase-change materials and their potential applications in sensing and microelectromechanical devices.

KEYWORDS: vanadium dioxide, strain engineering, carrier dynamics, phase transition, *s*-SNOM

INTRODUCTION

The interplay between strongly correlated electrons and lattice distortion facilitates the well-known metal–insulator transition (MIT) in vanadium dioxide (VO_2).^{1–3} With an accessible transition temperature of $T_c \approx 341$ K, VO_2 can be used as a thermochromic material in smart windows, solar reflectors, and detectors to realize flexible thermal management and temperature sensing.^{4–8} The phase transition in VO_2 can also be triggered by optical, electric, and magnetic stimulations,⁹ which enables a broad range of photonic and optoelectronic devices, such as photodetectors,¹⁰ field-effect transistors,^{11,12} tunable dielectric metasurfaces,^{13,14} optical control devices,^{15,16} and memory devices.^{17–19}

Recent studies have shown that strain can be introduced to shift the transition temperature and enrich the phase diagram of VO_2 ,²⁰ leading to self-organized coexisting metallic–insulating domains.^{21–24} Such strain modulation of MIT has extended the applications of VO_2 in high-performance strain sensors,^{25,26} microelectromechanical systems,^{27–30} and tunable electro-optic devices.^{31,32}

Unraveling the MIT in VO_2 has relied on ultrafast optical probes and near-field microscopies to deconvolute the coupled

electron–lattice dynamics and visualize nanoscale phase transition phenomena.^{33–38} Scattering-type scanning near-field optical microscopy (*s*-SNOM) has mapped the stress-tuned periodic domain patterns in VO_2 microcrystals,³⁹ while the combination of transient measurements with near-field imaging has revealed the ultrafast dynamics and phase inhomogeneities associated with MIT.⁴⁰ However, directly visualizing the strain-tuned coexistence of metallic and insulating phases at the nanoscale and their associated carrier dynamics remains an outstanding challenge.

In this work, we study the strain-modulated phases and carrier dynamics in bent VO_2 nanobeams. We demonstrate the near-field imaging of alternating insulating–metallic phase domains with nanoscale spatial resolution. With the integration

Received: May 7, 2024

Revised: July 9, 2024

Accepted: July 10, 2024

Published: July 17, 2024



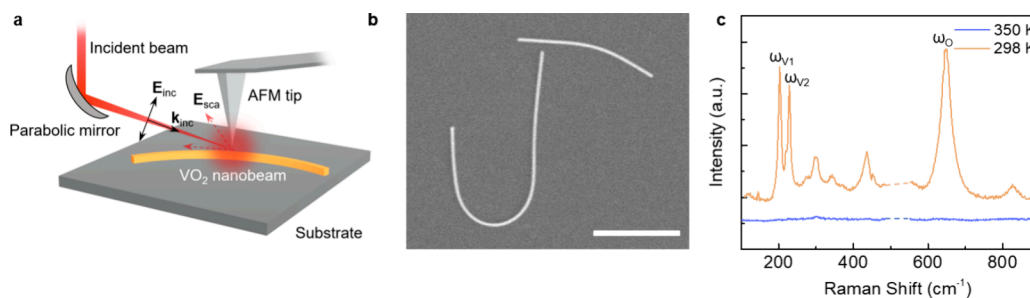


Figure 1. Experiment setup and materials characterization: (a) Schematic of the s-SNOM setup. (b) SEM images of bent VO₂ nanobeams. (c) Raman spectra of a VO₂ nanobeam measured below (298 K) and above (350 K) the phase transition temperature. Scale bar: 10 μm.

of visible-near-infrared pump–probe diagnostics,^{41,42} we further investigate the photocarrier dynamics in different phases within the VO₂ nanobeam. Our results provide insights into the phase inhomogeneities and carrier dynamics in strained VO₂ nanostructures that are pertinent to the development of advanced sensing and microelectromechanical devices.

RESULTS AND DISCUSSION

Figure 1a shows the schematic of our s-SNOM setup (see Methods for more details).^{43,44} The use of an atomic force microscope (AFM) tip enables the imaging of phase domains in VO₂ with a subdiffraction-limit spatial resolution. An 800 nm femtosecond laser beam is directed to the tip, where the near-field coupling between the tip apex and the nanobeam modulates the backscattered light to probe the local material properties. The VO₂ nanobeams in our experiments are synthesized by a vapor transport method⁴⁵ and mechanically transferred to the substrate. During this process, some nanobeams will naturally bend due to the uniaxial strain. The bent VO₂ nanobeams are clearly visualized by the high-resolution scanning electron microscope (SEM) image (Figure 1b). Figure 1c shows the Raman spectra of a VO₂ nanobeam measured below (298 K) and above (350 K) the transition temperature. The representative ω_{V_1} , ω_{V_2} , and ω_O phonon modes can be identified for the insulating VO₂, while the metallic VO₂ shows negligible Raman signals (Figure 1c).^{24,46}

We first conducted near-field imaging of a bent VO₂ nanobeam by scanning the sample underneath the AFM tip. Figure 2a shows the AFM topography of the nanobeam, and

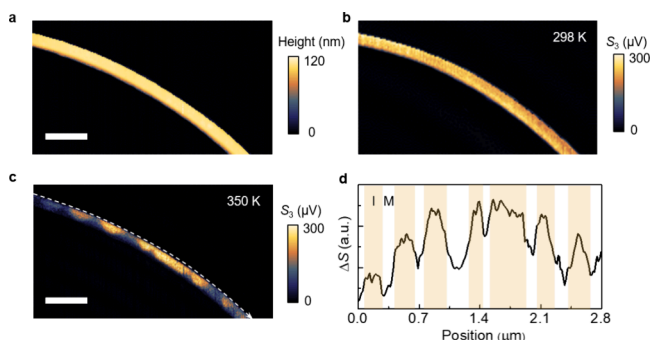


Figure 2. Near-field nanoimaging of phase domains. (a) AFM image of a bent VO₂ nanobeam. (b,c) s-SNOM images measured at (b) 298 and (c) 350 K. (d) Line profile of the near-field amplitude extracted from (c) along the centerline of the nanobeam, indicating coexisting insulating (I) and metallic (M) phases. Scale bars: 500 nm.

Figure 2b,c shows the corresponding near-field images. At room temperature (298 K), the s-SNOM signal intensity does not exhibit spatial variation, indicating a uniform insulating phase (Figure 2b). When the temperature is elevated to 350 K, the near-field image shows an alternating triangular-shaped domain pattern, which represents the coexisting insulating and metallic phases (Figure 2c). The variation of the s-SNOM intensity can be clearly seen from the line profile extracted along the nanobeam (Figure 2d), where the bright and dark regions correspond to the insulating and metallic domains, respectively. These phase domains have a feature size of ~200 nm (Figure 2d), demonstrating sub-diffraction-limit spatial resolution of the near-field imaging. The formation of such alternating domain patterns is ascribed to the strain-induced shift of transition temperature T_c and the competition between the strain energy and domain-wall energy.^{20,21} With the linearly distributed strain along the radial direction of the bent VO₂ nanobeam, the insulating and metallic domains are of nanotriangular shape, as shown in Figure 2c.²³ We also repeated the measurement on other bent VO₂ nanobeams and observed similar alternating phase domains at elevated temperatures (Figure S1).

We then studied carrier dynamics in different domains by integrating pump–probe optics into the s-SNOM system (Figure 3a). A 400 nm pump beam and an 800 nm probe beam with controlled time delay are directed onto the AFM tip (see Methods for more details). The transient s-SNOM signal is collected in different phase regions at both room and elevated temperatures (Figure 3b, c). The near-field amplitude showcases a striking increase after pump beam excitation due to the photoexcited carrier injection, followed by a signal decay that is attributed to carrier recombination and diffusion processes.⁴⁷ While there is no notable difference between the insulating phases at 298 and 350 K, the decay of s-SNOM intensity in the metallic phase (350 K) appears to be slower (Figure 3c). Additional experiments are also conducted to confirm the results (Figure S2).

To quantitatively understand the carrier behaviors, we calculate the carrier density-dependent dielectric function of both the metallic and insulating VO₂ by the Drude–Lorentz model (Figure S3):⁴⁷

$$\epsilon(\omega, \Delta t) = \epsilon_\infty + \sum_{j=1}^n \frac{f_j \omega_j^2}{\omega_j^2 - \omega^2 - i\omega\Gamma_j} - \frac{N(\Delta t)e^2}{m\epsilon_0} \frac{1}{\omega^2 + i\omega\Gamma_d} \quad (1)$$

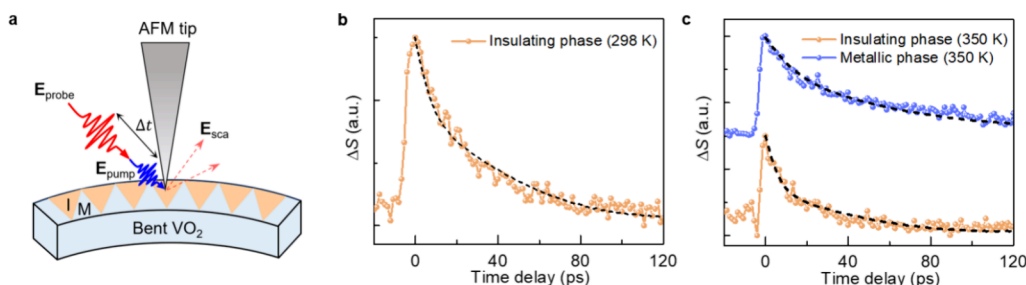


Figure 3. Transient measurements on VO₂ nanobeams: (a) Schematic of pump–probe s-SNOM experiment, (b) transient s-SNOM signal and fitting curve (dashed line) on a bent VO₂ nanobeam at 298 K, (c) normalized transient s-SNOM signals and fitting curves (dashed lines) on the same VO₂ nanobeam at 350 K, in both insulating and metallic domains. Two curves are offset from each other for better visualization.

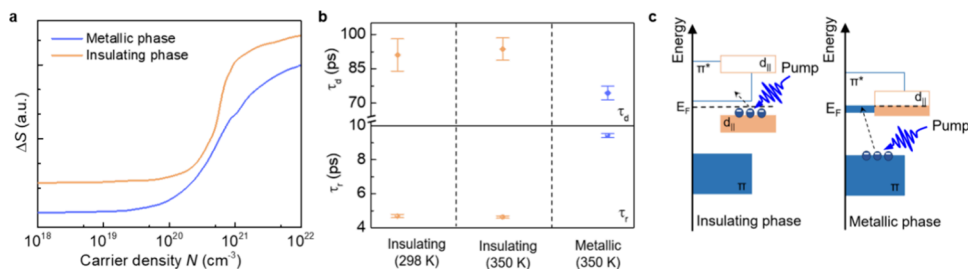


Figure 4. Carrier dynamics in VO₂ nanobeams. (a) Simulated s-SNOM intensity of the metallic and insulating phases of VO₂ nanobeams as a function of carrier density. (b) Fitted time constants for both phases. τ_r and τ_d represent the recombination and diffusion processes, respectively. (c) Band structures of insulating and metallic VO₂.

where ϵ_∞ is the background dielectric function, the second term stands for the contribution from the Lorentz oscillators, and the third term represents the contribution from the free carriers. f_j , ω_j , and Γ_j are the strength, frequency, and damping rate of the j th oscillator, ω represents the probe beam frequency, $N(\Delta t)$ is photoexcited electron density at the time delay of Δt , e , and m is the elementary charge and effective mass of the electron, ϵ_0 is the vacuum permittivity, and $\Gamma_d = \frac{e}{m\mu}$, where μ is the carrier mobility. Then, we conduct the finite-domain time difference (FDTD) simulation to calculate the near-field amplitude as a function of carrier density (see Methods and Figure S4 for more details).⁴⁸ The s-SNOM intensity at different carrier densities for both the metallic and insulating phases is plotted in Figure 4a.

The carrier density after pump excitation can be modeled to follow a bi-exponential decay, taking both the electron–hole recombination and carrier diffusion into consideration:⁴⁹

$$N(\Delta t) = N_0(A_r e^{-\Delta t/\tau_r} + A_d e^{-\Delta t/\tau_d}) \quad (2)$$

where N_0 is the initial carrier density after the excitation, Δt is the time delay, τ_r and τ_d are time constants that represent the recombination and diffusion process, respectively, and A_r and A_d are two coefficients with $A_r + A_d = 1$. By coupling eq 2 to 1 as well as the ΔS – N relation shown in Figure 4a, we could fit the transient data (Figure 3b,c) and obtain the parameters in eq 2. The fitted time constants are plotted in Figure 4b and other parameters are summarized in Table S1.

Metallic and insulating phases of VO₂ display distinct carrier dynamics. Considering the carrier recombination is usually faster than the diffusion process,⁵⁰ we assign the shorter time constant to τ_r and the longer time constant as τ_d . The electron–hole recombination after pump excitation in the metallic phase is slower than that in the insulating phase, followed by a slightly faster carrier diffusion process (Figure 4b). The slower carrier diffusion in the insulating phase can be

explained by the strong Coulomb repulsion in the correlated insulator that limits the freedom of carrier movements.^{11,37} For the opposite behavior in carrier recombination, we tentatively attribute it to phonon softening. Figure 4c shows the band structures of both phases. When VO₂ transits from the monoclinic insulating to the rutile metallic phase, the two separate $d_{||}$ bands degenerate to one $d_{||}$ band, coming in contact with the π^* band (Figure 4c).^{51,52} The carrier recombination in the insulating phase mainly happens between the lower $d_{||}$ band and the π^* band. In our experiments, the metallic phase also exhibits semiconducting characteristics because our pump beam has sufficient photon energy (~ 3.1 eV) to excite the electrons in the lower π band, leading to the electron–hole recombination between the π^* and π band (Figure 4c). The phonon-assisted nonradiative carrier recombination dynamics in VO₂ is inversely related to the strength of the electron–phonon coupling $\lambda\langle\omega^2\rangle$, where ω is the phonon frequency and λ is the dimensionless electron–phonon coupling constant.^{53,54} With softer phonon modes and lower phonon density of states,^{1,55,56} the metallic VO₂ has a smaller $\lambda\langle\omega^2\rangle$, leading to a larger recombination lifetime compared to the insulating VO₂.

CONCLUSIONS

In conclusion, we report the near-field imaging of nanoscale structural phases in strained VO₂ nanobeams and characterize the carrier dynamics in different phase domains. By coupling near-field experiments and FDTD simulations, we observe slower carrier diffusion and a shorter recombination lifetime in the insulating phase, which can be possibly explained by the strongly correlated electrons and different band structures between the two phases. Our results can help advance the understanding of strain-modulated phase structures in VO₂ for microelectromechanical devices and carrier dynamics in correlated materials.

METHODS

Materials and Characterizations. The VO₂ nanobeams were prepared by a vapor transport method.⁴⁵ Raman spectroscopy was conducted by a Renishaw micro-Raman measurement system, and the excitation wavelength is 532 nm. The SEM images were taken with an FEI Quanta 650 SEM system.

Experimental Setup. The near-field imaging of the VO₂ nanobeams is taken through a commercial s-SNOM system (Molecular Vista), and an 800 nm femtosecond laser (Spectra-Physics Tsunami 3941-30-M1S) is used as the light source. The 400 nm pump beam is generated by passing part of the 800 nm laser through a beta barium borate crystal (Eksma Optics). The laser fluence in our experiments is $\sim 9.3 \mu\text{J}/\text{cm}^2$, which is much lower than the threshold fluence of photo-induced phase transition reported by previous studies.^{57,58} A delay stage (Thorlabs) is used to control the time delay between the pump and probe beam. The pump beam is modulated by an acoustic optical modulator (AOM, Thorlabs) at the third harmonic AFM tip oscillation frequency. A parabolic mirror is used to direct the pump and probe beams to the tip-sample system, and the backscattered probe beam is collected by an avalanche photodiode (Thorlabs). The near-field signal is obtained after the far-field noise is suppressed through a demodulation process at the AOM modulation frequency by a lock-in amplifier.

FDTD Simulations. Numerical simulations were performed using commercial software Ansys Lumerical based on the finite-domain time difference (FDTD) method. The nanobeam is modeled as a curved solid with a square cross-section area (side length 200 nm), and the AFM tip is modeled as a cone with its apex rounded by a sphere (radius 20 nm) (Figure S4). An 800 nm plane wave is used to illuminate the system, and a field monitor is used to collect the backscattered light. The near-field signal is obtained by the modulation and demodulation process with the method we have developed before.⁴⁸ Briefly, we model the AFM tip to oscillate periodically above the sample at a specific frequency ($\Omega \sim 250$ kHz), where the tip-sample distance h varies between 2 and 62 nm with time by $h = 32 - 30 \cos(2\pi\Omega t)$. We then simulate the scattered light intensity $S(t_i)$ at N discrete h_i and mimic the demodulation process in the s-SNOM experiments to suppress the far-field noise and extract the near-field amplitude ΔS by applying a Fourier integral at the third harmonic frequency ($k = 3$):

$$\Delta S = \sum_{i=1}^N S(t_i) e^{-i2k\pi\Omega t_i} (t_{i+1} - t_i)$$

where t_i is the time that corresponds to each h_i . By repeating this simulation procedure based on the dielectric function at different carrier densities calculated from eq 1, the ΔS - N relation in Figure 4a can be obtained.

ASSOCIATED CONTENT

Supporting Information

The Supporting Information is available free of charge at <https://pubs.acs.org/doi/10.1021/acsp Photonics.4c00848>.

AFM topography and s-SNOM image of a bent VO₂ nanobeam, time-resolved measurements on a strained VO₂ nanobeam, calculated dielectric function of VO₂ in the metallic and insulating phase, schematic of FDTD

simulation, and fitting results of the transient s-SNOM signal (PDF)

AUTHOR INFORMATION

Corresponding Authors

Jingang Li – Laser Thermal Laboratory, Department of Mechanical Engineering, University of California, Berkeley, California 94720, United States; orcid.org/0000-0003-0827-9758; Email: jingang@berkeley.edu

Junqiao Wu – Department of Materials Science and Engineering, University of California, Berkeley, California 94720, United States; orcid.org/0000-0002-1498-0148; Email: wuj@berkeley.edu

Costas P. Grigoropoulos – Laser Thermal Laboratory, Department of Mechanical Engineering, University of California, Berkeley, California 94720, United States; orcid.org/0000-0002-8505-4037; Email: cgrigoro@berkeley.edu

Authors

Rundi Yang – Laser Thermal Laboratory, Department of Mechanical Engineering, University of California, Berkeley, California 94720, United States; orcid.org/0000-0002-2877-939X

Yuhang Cai – Department of Materials Science and Engineering, University of California, Berkeley, California 94720, United States

Brian W. Blankenship – Laser Thermal Laboratory, Department of Mechanical Engineering, University of California, Berkeley, California 94720, United States; orcid.org/0000-0003-4212-6835

Complete contact information is available at: <https://pubs.acs.org/10.1021/acsp Photonics.4c00848>

Author Contributions

[§]R.Y. and J.L. contributed equally to this work.

Funding

C.P.G. acknowledges the financial support from Laser Primitives under the DOE SBIR Phase 2 grant DE-SC0018461. J.W. acknowledges support by the U.S. Department of Energy, Office of Science, Office of Basic Energy Sciences, Materials Sciences and Engineering Division under contract no. DE-AC02-05CH11231 (Electronic Materials program).

Notes

The authors declare no competing financial interest.

REFERENCES

- (1) Liu, K.; Lee, S.; Yang, S.; Delaire, O.; Wu, J. Recent progresses on physics and applications of vanadium dioxide. *Mater. Today* **2018**, *21*, 875–896.
- (2) Weber, C.; O'Regan, D. D.; Hine, N. D. M.; Payne, M. C.; Kotliar, G.; Littlewood, P. B. Vanadium Dioxide: A Peierls-Mott Insulator Stable against Disorder. *Phys. Rev. Lett.* **2012**, *108*, No. 256402.
- (3) Biermann, S.; Poteryaev, A.; Lichtenstein, A. I.; Georges, A. Dynamical Singlets and Correlation-Assisted Peierls Transition in VO₂. *Phys. Rev. Lett.* **2005**, *94*, No. 026404.
- (4) Ke, Y.; Zhou, C.; Zhou, Y.; Wang, S.; Chan, S. H.; Long, Y. Emerging Thermal-Responsive Materials and Integrated Techniques Targeting the Energy-Efficient Smart Window Application. *Adv. Funct. Mater.* **2018**, *28*, No. 1800113.

- (5) Gao, Y.; Luo, H.; Zhang, Z.; Kang, L.; Chen, Z.; Du, J.; Kanehira, M.; Cao, C. Nanoceramic VO₂ thermochromic smart glass: A review on progress in solution processing. *Nano Energy* **2012**, *1*, 221–246.
- (6) Tang, K.; Dong, K.; Li, J.; Gordon, M. P.; Reichertz, F. G.; Kim, H.; Rho, Y.; Wang, Q.; Lin, C.-Y.; Grigoropoulos, C. P.; et al. Temperature-adaptive radiative coating for all-season household thermal regulation. *Science* **2021**, *374*, 1504–1509.
- (7) Sun, K.; Riedel, C. A.; Urbani, A.; Simeoni, M.; Mengali, S.; Zalkovskij, M.; Bilenberg, B.; de Groot, C. H.; Muskens, O. L. VO₂ Thermochromic Metamaterial-Based Smart Optical Solar Reflector. *ACS Photonics* **2018**, *5*, 2280–2286.
- (8) Hu, R.; Xi, W.; Liu, Y.; Tang, K.; Song, J.; Luo, X.; Wu, J.; Qiu, C.-W. Thermal camouflaging metamaterials. *Mater. Today* **2021**, *45*, 120–141.
- (9) Ke, Y.; Wang, S.; Liu, G.; Li, M.; White, T. J.; Long, Y. Vanadium Dioxide: The Multistimuli Responsive Material and Its Applications. *Small* **2018**, *14*, No. 1802025.
- (10) Li, Z.; Hu, Z.; Peng, J.; Wu, C.; Yang, Y.; Feng, F.; Gao, P.; Yang, J.; Xie, Y. Ultrahigh Infrared Photoresponse from Core–Shell Single-Domain-VO₂/V₂O₅ Heterostructure in Nanobeam. *Adv. Funct. Mater.* **2014**, *24*, 1821–1830.
- (11) Nakano, M.; Shibuya, K.; Okuyama, D.; Hatano, T.; Ono, S.; Kawasaki, M.; Iwasa, Y.; Tokura, Y. Collective bulk carrier delocalization driven by electrostatic surface charge accumulation. *Nature* **2012**, *487*, 459–462.
- (12) Sengupta, S.; Wang, K.; Liu, K.; Bhat, A. K.; Dhara, S.; Wu, J.; Deshmukh, M. M. Field-effect modulation of conductance in VO₂ nanobeam transistors with HfO₂ as the gate dielectric. *Appl. Phys. Lett.* **2011**, *99*, No. 062114.
- (13) Shu, F. Z.; Wang, J. N.; Peng, R. W.; Xiong, B.; Fan, R. H.; Gao, Y. J.; Liu, Y.; Qi, D. X.; Wang, M. Electrically Driven Tunable Broadband Polarization States via Active Metasurfaces Based on Joule-Heat-Induced Phase Transition of Vanadium Dioxide. *Laser Photonics Rev.* **2021**, *15*, No. 2100155.
- (14) Tripathi, A.; John, J.; Kruk, S.; Zhang, Z.; Nguyen, H. S.; Berguiga, L.; Romeo, P. R.; Orobtochouk, R.; Ramanathan, S.; Kivshar, Y.; et al. Tunable Mie-Resonant Dielectric Metasurfaces Based on VO₂ Phase-Transition Materials. *ACS Photonics* **2021**, *8*, 1206–1213.
- (15) Shu, F. Z.; Yu, F. F.; Peng, R. W.; Zhu, Y. Y.; Xiong, B.; Fan, R. H.; Wang, Z. H.; Liu, Y.; Wang, M. Dynamic Plasmonic Color Generation Based on Phase Transition of Vanadium Dioxide. *Adv. Opt. Mater.* **2018**, *6*, No. 1700939.
- (16) Jia, Z.-Y.; Shu, F.-Z.; Gao, Y.-J.; Cheng, F.; Peng, R.-W.; Fan, R.-H.; Liu, Y.; Wang, M. Dynamically Switching the Polarization State of Light Based on the Phase Transition of Vanadium Dioxide. *Phys. Rev. Applied* **2018**, *9*, No. 034009.
- (17) Blankenship, B. W.; Li, R.; Guo, R.; Zhao, N.; Shin, J.; Yang, R.; Ko, S. H.; Wu, J.; Rho, Y.; Grigoropoulos, C. Photothermally Activated Artificial Neuromorphic Synapses. *Nano Lett.* **2023**, *23*, 9020–9025.
- (18) Bae, S. H.; Lee, S.; Koo, H.; Lin, L.; Jo, B. H.; Park, C.; Wang, Z. L. The Memristive Properties of a Single VO₂ Nanowire with Switching Controlled by Self-Heating. *Adv. Mater.* **2013**, *25*, 5098–5103.
- (19) Driscoll, T.; Kim, H.-T.; Chae, B.-G.; Kim, B.-J.; Lee, Y.-W.; Jocker, N. M.; Palit, S.; Smith, D. R.; Di Ventra, M.; Basov, D. N. Memory Metamaterials. *Science* **2009**, *325*, 1518–1521.
- (20) Park, J. H.; Coy, J. M.; Kasirga, T. S.; Huang, C.; Fei, Z.; Hunter, S.; Cobden, D. H. Measurement of a solid-state triple point at the metal–insulator transition in VO₂. *Nature* **2013**, *500*, 431–434.
- (21) Wu, J.; Gu, Q.; Guiton, B. S.; De Leon, N. P.; Ouyang, L.; Park, H. Strain-Induced Self Organization of Metal–Insulator Domains in Single-Crystalline VO₂ Nanobeams. *Nano Lett.* **2006**, *6*, 2313–2317.
- (22) Wei, J.; Wang, Z.; Chen, W.; Cobden, D. H. New aspects of the metal–insulator transition in single-domain vanadium dioxide nanobeams. *Nat. Nanotechnol.* **2009**, *4*, 420–424.
- (23) Cao, J.; Ertekin, E.; Srinivasan, V.; Fan, W.; Huang, S.; Zheng, H.; Yim, J. W. L.; Khanal, D. R.; Ogletree, D. F.; Grossman, J. C.; et al. Strain engineering and one-dimensional organization of metal–insulator domains in single-crystal vanadium dioxide beams. *Nat. Nanotechnol.* **2009**, *4*, 732–737.
- (24) Shi, R.; Chen, Y.; Cai, X.; Lian, Q.; Zhang, Z.; Shen, N.; Amini, A.; Wang, N.; Cheng, C. Phase management in single-crystalline vanadium dioxide beams. *Nat. Commun.* **2021**, *12*, 4214.
- (25) Hu, B.; Ding, Y.; Chen, W.; Kulkarni, D.; Shen, Y.; Tsukruk, V. V.; Wang, Z. L. External-Strain Induced Insulating Phase Transition in VO₂ Nanobeam and Its Application as Flexible Strain Sensor. *Adv. Mater.* **2010**, *22*, 5134–5139.
- (26) Hu, B.; Zhang, Y.; Chen, W.; Xu, C.; Wang, Z. L. Self-heating and External Strain Coupling Induced Phase Transition of VO₂ Nanobeam as Single Domain Switch. *Adv. Mater.* **2011**, *23*, 3536–3541.
- (27) Dong, K.; Choe, H. S.; Wang, X.; Liu, H.; Saha, B.; Ko, C.; Deng, Y.; Tom, K. B.; Lou, S.; Wang, L. A 0.2 V Micro-Electromechanical Switch Enabled by a Phase Transition. *Small* **2018**, *14*, No. 1703621.
- (28) Wang, K.; Cheng, C.; Cardona, E.; Guan, J.; Liu, K.; Wu, J. Performance Limits of Microactuation with Vanadium Dioxide as a Solid Engine. *ACS Nano* **2013**, *7*, 2266–2272.
- (29) Dong, K.; Lou, S.; Choe, H. S.; Liu, K.; You, Z.; Yao, J.; Wu, J. Stress compensation for arbitrary curvature control in vanadium dioxide phase transition actuators. *Appl. Phys. Lett.* **2016**, *109*, No. 023504.
- (30) Parikh, P.; Chakraborty, C.; Abhilash, T. S.; Sengupta, S.; Cheng, C.; Wu, J.; Deshmukh, M. M. Dynamically Tracking the Strain Across the Metal–Insulator Transition in VO₂ Measured Using Electromechanical Resonators. *Nano Lett.* **2013**, *13*, 4685–4689.
- (31) Lee, D.; Lee, J.; Song, K.; Xue, F.; Choi, S.-Y.; Ma, Y.; Podkaminer, J.; Liu, D.; Liu, S.-C.; Chung, B.; et al. Sharpened VO₂ Phase Transition via Controlled Release of Epitaxial Strain. *Nano Lett.* **2017**, *17*, 5614–5619.
- (32) Wang, X.; Dong, K.; Choe, H. S.; Liu, H.; Lou, S.; Tom, K. B.; Bechtel, H. A.; You, Z.; Wu, J.; Yao, J. Multifunctional Microelectro-Opto-mechanical Platform Based on Phase-Transition Materials. *Nano Lett.* **2018**, *18*, 1637–1643.
- (33) Jager, M. F.; Ott, C.; Kraus, P. M.; Kaplan, C. J.; Pouse, W.; Marvel, R. E.; Haglund, R. F.; Neumark, D. M.; Leone, S. R. Tracking the insulator-to-metal phase transition in VO₂ with few-femtosecond extreme UV transient absorption spectroscopy. *P. Natl. Acad. Sci. U.S.A.* **2017**, *114*, 9558–9563.
- (34) Sternbach, A. J.; Ruta, F. L.; Shi, Y.; Slusar, T.; Schalch, J.; Duan, G.; McLeod, A. S.; Zhang, X.; Liu, M.; Millis, A. J.; et al. Nanotextured Dynamics of a Light-Induced Phase Transition in VO₂. *Nano Lett.* **2021**, *21*, 9052–9060.
- (35) Xu, J.; Chen, D.; Meng, S. Decoupled ultrafast electronic and structural phase transitions in photoexcited monoclinic VO₂. *Sci. Adv.* **2022**, *8*, No. eadd2392.
- (36) Liu, M.; Hwang, H. Y.; Tao, H.; Strikwerda, A. C.; Fan, K.; Keiser, G. R.; Sternbach, A. J.; West, K. G.; Kittiwatanakul, S.; Lu, J.; et al. Terahertz-field-induced insulator-to-metal transition in vanadium dioxide metamaterial. *Nature* **2012**, *487*, 345–348.
- (37) Qazilbash, M. M.; Brehm, M.; Chae, B.-G.; Ho, P.-C.; Andreev, G. O.; Kim, B.-J.; Yun, S. J.; Balatsky, A. V.; Maple, M. B.; Keilmann, F.; et al. Mott Transition in VO₂ Revealed by Infrared Spectroscopy and Nano-Imaging. *Science* **2007**, *318*, 1750–1753.
- (38) Dönges, S. A.; Khatib, O.; O’Callahan, B. T.; Atkin, J. M.; Park, J. H.; Cobden, D.; Raschke, M. B. Ultrafast Nanoimaging of the Photoinduced Phase Transition Dynamics in VO₂. *Nano Lett.* **2016**, *16*, 3029–3035.
- (39) Jones, A. C.; Berweger, S.; Wei, J.; Cobden, D.; Raschke, M. B. Nano-optical Investigations of the Metal–Insulator Phase Behavior of Individual VO₂ Microcrystals. *Nano Lett.* **2010**, *10*, 1574–1581.
- (40) Huber, M. A.; Plankl, M.; Eisele, M.; Marvel, R. E.; Sandner, F.; Korn, T.; Schüller, C.; Haglund, R. F.; Huber, R.; Cocker, T. L. Ultrafast Mid-Infrared Nanoscopy of Strained Vanadium Dioxide Nanobeams. *Nano Lett.* **2016**, *16*, 1421–1427.

- (41) Li, J.; Yang, R.; Rho, Y.; Ci, P.; Eliceiri, M.; Park, H. K.; Wu, J.; Grigoropoulos, C. P. Ultrafast Optical Nanoscopy of Carrier Dynamics in Silicon Nanowires. *Nano Lett.* **2023**, *23*, 1445–1450.
- (42) Li, J.; Yang, R.; Higashitarumizu, N.; Dai, S.; Wu, J.; Javey, A.; Grigoropoulos, C. P. Transient Nanoscopy of Exciton Dynamics in 2D Transition Metal Dichalcogenides. *Adv. Mater.* **2024**, *36*, 2311568.
- (43) Li, J.; Yang, R.; Yao, K.; Huang, Y.; Rho, Y.; Fan, D. E.; Zheng, Y.; Grigoropoulos, C. P. Near-Field Nanoimaging of Colloidal Transition Metal Dichalcogenide Waveguides. *Adv. Funct. Mater.* **2024**, *34*, 2312127.
- (44) Liu, Y.; Li, J.; Zhu, Y.; Ai, Q.; Xu, R.; Yang, R.; Zhang, B.; Fang, Q.; Zhai, T.; Xu, C.; et al. Spatially Resolved Anion Diffusion and Tunable Waveguides in Bismuth Halide Perovskites. *Nano Lett.* **2024**, *24*, 5182–5188.
- (45) Guiton, B. S.; Gu, Q.; Prieto, A. L.; Gudiksen, M. S.; Park, H. Single-Crystalline Vanadium Dioxide Nanowires with Rectangular Cross Sections. *J. Am. Chem. Soc.* **2005**, *127*, 498–499.
- (46) Atkin, J. M.; Berweger, S.; Chavez, E. K.; Raschke, M. B.; Cao, J.; Fan, W.; Wu, J. Strain and temperature dependence of the insulating phases of VO₂ near the metal-insulator transition. *Phys. Rev. B* **2012**, *85*, No. 020101(R).
- (47) Verleur, H. W.; Barker, A. S.; Berglund, C. N. Optical Properties of VO₂ between 0.25 and 5 eV. *Phys. Rev.* **1968**, *172*, 788–798.
- (48) Yang, R.; Li, J.; Grigoropoulos, C. P. Numerical Study of Carrier Dynamics in Pump–Probe Near-Field Nanoscopy. *J. Phys. Chem. C* **2024**, *128*, 261–267.
- (49) Wall, S.; Foglia, L.; Wegkamp, D.; Appavoo, K.; Nag, J.; Haglund, R. F.; Stähler, J.; Wolf, M. Tracking the evolution of electronic and structural properties of VO₂ during the ultrafast photoinduced insulator-metal transition. *Phys. Rev. B* **2013**, *87*, No. 115126.
- (50) Gabriel, M. M.; Kirschbrown, J. R.; Christesen, J. D.; Pinion, C. W.; Zigler, D. F.; Grumstrup, E. M.; Mehl, B. P.; Cating, E. E. M.; Cahoon, J. F.; Papanikolas, J. M. Direct Imaging of Free Carrier and Trap Carrier Motion in Silicon Nanowires by Spatially-Separated Femtosecond Pump–Probe Microscopy. *Nano Lett.* **2013**, *13*, 1336–1340.
- (51) O’Callahan, B. T.; Jones, A. C.; Hyung Park, J.; Cobden, D. H.; Atkin, J. M.; Raschke, M. B. Inhomogeneity of the ultrafast insulator-to-metal transition dynamics of VO₂. *Nat. Commun.* **2015**, *6*, 6849.
- (52) Liu, H.-W.; Liu, W.-H.; Suo, Z.-J.; Wang, Z.; Luo, J.-W.; Li, S.-S.; Wang, L.-W. Unifying the order and disorder dynamics in photoexcited VO₂. *P. Natl. Acad. Sci. U. S. A.* **2022**, *119*, No. e2122534119.
- (53) Ji, Y.; Cheng, L.; Li, N.; Yuan, Y.; Liang, W.; Yang, H. Decoupling between metal–insulator transition and structural phase transition in an interface-engineered VO₂. *J. Phys.: Condens. Matter* **2021**, *33*, No. 105603.
- (54) Gadermaier, C.; Alexandrov, A. S.; Kabanov, V. V.; Kusar, P.; Mertelj, T.; Yao, X.; Manzoni, C.; Brida, D.; Cerullo, G.; Mihailovic, D. Electron-Phonon Coupling in High-Temperature Cuprate Superconductors Determined from Electron Relaxation Rates. *Phys. Rev. Lett.* **2010**, *105*, No. 257001.
- (55) Budai, J. D.; Hong, J.; Manley, M. E.; Specht, E. D.; Li, C. W.; Tischler, J. Z.; Abernathy, D. L.; Said, A. H.; Leu, B. M.; Boatner, L. A.; et al. Metallization of vanadium dioxide driven by large phonon entropy. *Nature* **2014**, *515*, 535–539.
- (56) Wall, S.; Yang, S.; Vidas, L.; Chollet, M.; Glowonia, J. M.; Kozina, M.; Katayama, T.; Henighan, T.; Jiang, M.; Miller, T. A.; et al. Ultrafast disordering of vanadium dimers in photoexcited VO₂. *Science* **2018**, *362*, 572–576.
- (57) Sternbach, A. J.; Slusar, T.; Ruta, F. L.; Moore, S.; Chen, X.; Liu, M. K.; Kim, H. T.; Millis, A. J.; Averitt, R. D.; Basov, D. N. Inhomogeneous Photosusceptibility of VO₂ Films at the Nanoscale. *Phys. Rev. Lett.* **2024**, *132*, No. 186903.
- (58) Lysenko, S.; Kumar, N.; Rúa, A.; Figueroa, J.; Lu, J.; Fernández, F. Ultrafast structural dynamics of VO₂. *Phys. Rev. B* **2017**, *96*, No. 075128.